Tightly bound states in a uniform field with asymmetric tunneling

Huan-Yu Wang [1,*] and Wu-Ming Liu[2]

[1]*Department of Physics, Fuzhou University, Fuzhou 350108, China*
[2]*Beijing National Laboratory for Condensed Matter Physics, Institute of Physics, Chinese Academy of Sciences, Beijing 100190, China*

We investigate the localization behavior of the non-Hermitian tightly bound state in the presence of asymmetric tunneling and external uniform fields in various dimensions, where the discrete translational symmetry and the inversion symmetry are broken. We demonstrate that the non-Hermitian skin effects can still exist and compete with Wannier-Stark localization induced by the uniform fields. The total localization is not only related to the size of the system, but the net tunneling strength as well. For the two-dimensional lattices with square shape boundaries, the uniform fields can pull back the population of the states at the corner and the fading stripe localization can be observed as a compromise between the two-dimensional non-Hermitian skin effects and the uniform fields. The experimental simulation of the non-Hermitian chain with uniform fields can be achieved by the methods of electrical circuits.

I. INTRODUCTION

The open quantum systems with gain-loss or asymmetric tunneling feature non-Hermiticity and have been attracting increasing interests over the years [1–16]. One extraordinary property of the non-Hermitian lattice model lies in the localization behavior that not only the edge modes, but also all the bulk states can pile up at one end of the lattice, which is known as the non-Hermitian skin effect (NHSE) [17–38]. In correspondence, the non-Bloch band theory was developed for topological characterizations and to retain bulk-boundary correspondence in the lattices with the NHSE, the Bloch wave vector is expanded to be complex, which lies in the generalized Brillouin zone [39–48]. In addition, from a perspective of quantum transport, the NHSE can be topologically indicated by the loops formed the energy spectrum, which encloses the nonzero area in the complex plane [49,50].

Recently, studies on the NHSE were gradually expanded to the higher dimensions, where the asymmetric tunneling along diverse directions can drive the physical states to the corner [51–57]. Meanwhile, the shapes of the boundary can greatly affect the localization behavior. However, despite the achieved results so far, we observed that most of the research on the NHSE is restricted to the lattice systems with discrete translational symmetries and the skin-effect localization can be identified by the generalized Brillouin zone. It is natural to ask the following question: What is the localization behavior for non-Hermitian systems without the discrete translational symmetry in one and higher dimensions?

In this work, we develop a description of the non-Hermitian tightly bound states in various dimensions with the presence of external uniform fields and asymmetric tunneling, where the discrete translational symmetry, as well as the inversion symmetry, is broken. We demonstrate that the NHSE

can still exist despite the absence of the well-defined generalized Brillouin zone. Meanwhile, the NHSE can compete with Wannier-Stark localization induced by the uniform fields and the total localization behavior can be remarkable. Specifically, for one-dimensional systems ($d = 1$), Wannier-Stark localization takes the dominant place in the large field limit and the NHSE plays the leading role in the small field limit. When the uniform field is of moderate strength, the localization of the states not only depends on the size of the system but also the net tunneling strength.

For the two-dimensional lattices of square shape boundaries ($d = 2$), the external uniform fields can pull back the population of the states at the corner and the states of different energies are pulled back differently [58]. In this way, the fading stripe localization can be formed. Once the shapes of boundaries get changed, e.g., considering a boundary cut along the diagonal line of the square lattice, the localization center can be changed dramatically. Meanwhile, we also demonstrate how the uniform fields can destroy the exceptional points (EPs) and the parity-time symmetry no longer exists. In the last part of this paper, an experimental simulation of the non-Hermitian tightly bound states with external uniform fields is proposed via the methods of circuit lattices.

II. MODEL AND RESULTS

A. One-dimensional localization behavior

To consider the non-Hermitian system without discrete translational symmetries, we include the uniform fields in the quantum chain with asymmetric tunneling. The Hamiltonian can be characterized by

$$H = \sum_{j=1}^{N-1}(t_R c_{j+1}^\dagger c_j + t_L c_j^\dagger c_{j+1}) + \sum_{j=1}^{N} w j c_j^\dagger c_j, \qquad (1)$$

where $t_{R(L)} \in R$ denotes the tunneling to the right (left) nearest sites and N is the length of the quantum chain. The linearly
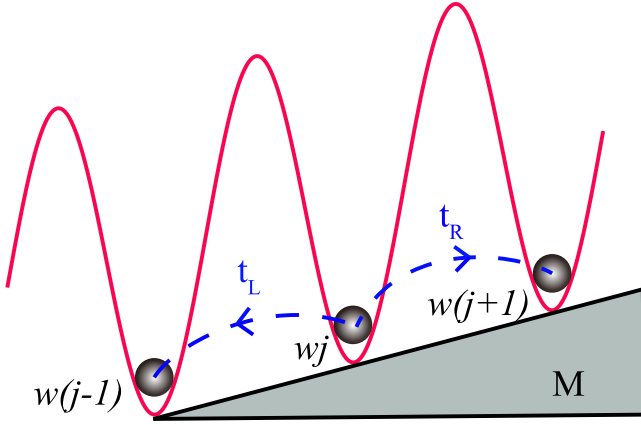
_____
*eurake27hywang@163.com

FIG. 1. The schematic presentation of the non-Hermitian tightly bound states with the external uniform field M. $t_L \neq t_R$ presents the asymmetric tunneling and w is the strength of the uniform field.

site-dependent potential wj depicts the presence of the uniform field M. A schematic picture of the system is shown in Fig. 1. For $t_R \neq t_L$, the model in Eq. (1) can be conceived as an expanded non-Hermitian Hatano-Nelson model [1,5,59–61]. In the limit of zero fields, the asymmetric tunneling between the periodic potentials can induce the NHSE and all the states are forced to be localized at one end of the lattice. However, if we consider the Hermitian cases with symmetric tunneling $t_R = t_L = t$, the energy spectrum forms the Wannier-Stark ladders in the case of large-enough external fields $w \gg t$. The state corresponding to the jth largest eigenenergy is localized at the jth site of the lattice. Such a localization is known as Wannier-Stark localization [62–66]. For a quantum chain of finite size, with moderate field strength, the NHSE can still exist and compete with Wannier-Stark localization. The exact form of the total population of the states can be cumbersome.

To present an analytical solution to the localization behavior, we assume an arbitrary single-particle state as

$$\psi = \sum_{l=1}^{l=N} \varphi_l c_l^\dagger |0\rangle, \tag{2}$$

where $|0\rangle$ denotes the fermion vacuum and φ_l is the wave function at each unit cell. Based on the Schrödinger equation $H\psi = E\psi$, the following recursion relation can be obtained [67–69]:

$$t_R \varphi_{l-1} + t_L \varphi_{l+1} + wl\varphi_l = E\varphi_l. \tag{3}$$

It shall be noticed that the asymmetric tunneling can be transformed to a symmetric one in the Hermitian model. In detail, considering a transformation S on the basis and obtain $\varphi_l = e^{\beta l} \Gamma_l$, Eq. (3) can change to the form

$$t_R e^{-\beta} \Gamma_{l-1} + t_L e^{\beta} \Gamma_{l+1} + wl\Gamma_l = E\Gamma_l. \tag{4}$$

If we keep $\beta = \ln \sqrt{\frac{t_R}{t_L}}$ and assign $t_0 = t_R e^{-\beta} = \sqrt{t_L t_R}$, the recurrence equation of the Hermitian chain with symmetric tunneling can be obtained

$$t_0(\Gamma_{l-1} + \Gamma_{l+1}) + wl\Gamma_l = E\Gamma_l. \tag{5}$$

Here, we prefer to regard the t_0 in the transformed Hermitian chain as the net tunneling since it is an intrinsic property

of the model in Eq. (1) and cannot make any changes to the NHSE. Before proceeding, we shall mention that the transformation S, which changes the basis $c_l^\dagger |0\rangle$ to $d_l^\dagger |0\rangle$ and $\psi = \sum_l \varphi_l c_l^\dagger |0\rangle = \sum_l \Gamma_l d_l^\dagger |0\rangle$, can be conceived as the Peierls substitution of the complex flux $i\beta$ [70]. The transformation S cannot change the real-space energy spectrum, but will contribute to differences in the localization behavior. Conventionally, given the recurrence relations in Eq. (5), the population of the state can be obtained through the transfer matrix approach, but for the model above with uniform fields, this can be difficult (see the Appendix). As a replacement, we utilize the recursion formula of the Bessel functions

$$Z_{\nu+1}(x) + Z_{\nu-1}(x) = \left(\frac{2\nu}{x}\right) Z_\nu(x), \tag{6}$$

where $Z_\nu(x)$ is the νth-order Bessel function and the solution to Γ_l can be depicted as

$$\Gamma_l = AJ_{l-\lambda\alpha}(2\alpha) + BY_{l-\lambda\alpha}(2\alpha), \tag{7}$$

where $J_\nu(x)$ and $Y_\nu(x)$ are the Bessel functions of the first and the second kinds with

$$\alpha = \frac{t_0}{w}, \lambda = \frac{E}{t_0}. \tag{8}$$

In correspondence, we have

$$\varphi_l = e^{\beta l} \left[AJ_{l-\frac{E}{W}} \left(\frac{2\sqrt{t_L t_R}}{w} \right) + BY_{l-\frac{E}{W}} \left(\frac{2\sqrt{t_L t_R}}{w} \right) \right]. \tag{9}$$

The coefficient $e^{\beta l}$ signifies the presence of NHSE despite the absence of discrete translational symmetry and the well-defined generalized Brillouin zone. In the large field limit

$$\tau = \frac{2\sqrt{t_L t_R}}{w} \to 0, \tag{10}$$

nonvanishing wave functions (φ_l) can only be obtained with $E = wl$, which is due to the numerical properties of the Bessel functions

$$|\lim_{x\to 0} J_\nu(x)| \neq 0, \quad \text{iff} \quad \nu = 0;$$
$$|\lim_{x\to 0} Y_\nu(x)| = \infty. \tag{11}$$

Hence, the Wannier-Stark-ladder-like energy spectrum can still be formed in the large field limit and the eigenstates are of Wannier-Stark localization. The effects of decaying (boosting) coefficient $e^{\beta l}$ are canceled by the normalization factor. In other words, Wannier-Stark localization can win over the NHSE in the large field limit.

In the low field limit, $\tau \to \infty$, the Bessel functions in Eqs. (7)–(9) have the asymptotic behavior

$$\lim_{\tau\to\infty} J_{l-\frac{E}{W}}(\tau) = \sqrt{\frac{2}{\pi\tau}} \cos\left(\tau - \frac{2(l-\frac{E}{W})+1}{4}\pi \right), \tag{12}$$

$$\lim_{\tau\to\infty} Y_{l-\frac{E}{W}}(\tau) = \sqrt{\frac{2}{\pi\tau}} \sin\left(\tau - \frac{2(l-\frac{E}{W})+1}{4}\pi \right). \tag{13}$$

According to Eqs. (7), (12), and (13), the wave function of the transformed Hermitian model can mimic the sinusoidal (or cosine) function in the low field limit, which is the Bloch wave under periodic boundary conditions and the corresponding
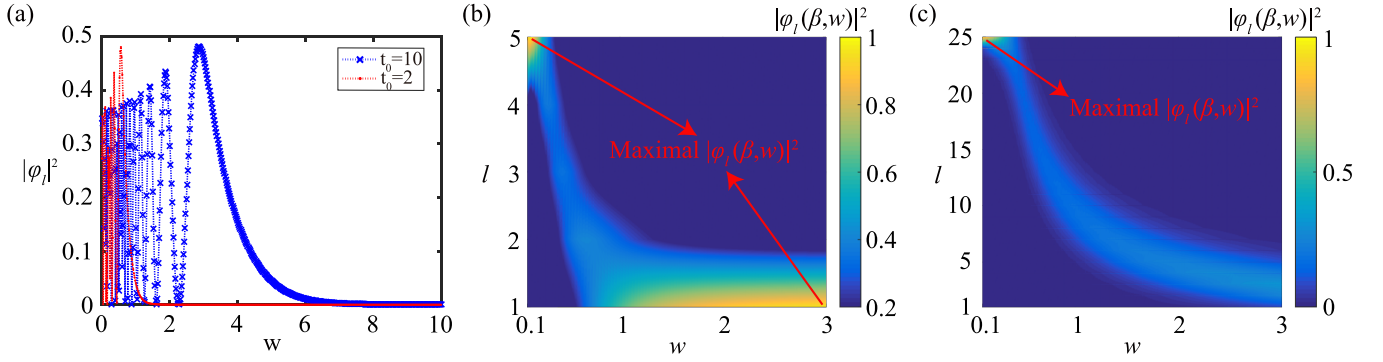
FIG. 2. (a) $|\varphi_l|^2$ as a function of the strength of the uniform field with fixed $\beta = 0.02$, $N = 5$, $l = 5$, and $t_0 = 2$ (10) for the red (blue) lines. With different net tunneling t_0, the maximum value of $|\varphi_l|^2$ happens with different external uniform field strength w. (b,c) $|\varphi_l(\beta, w)|^2$ as a function of w and l with fixed $t_0 = 0.5$. (b) For a finite chain of length $N = 5$ and $\beta = 1$, $|\varphi_l(\beta, w)|^2$ is maximally localized at $l = 1$ despite $e^{\beta} > 1$ when the strength of uniform field satisfies $w = 3$. (c) Enlarging the size of the chain and set $\beta = 3$, the NHSE takes the dominant place and $|\varphi_l(\beta, w)|^2$ is maximally localized at $l = N = 25$.

energy spectrum shall be periodic. Meanwhile, for Hermitian chains in the thermodynamic limit, the real-space energy spectrum with periodic boundary conditions (PBCs) coincides with that of the open boundary conditions (OBCs) [49]. As the transformation S cannot change the energy spectrum, the energy spectrum of the original non-Hermitian chain in Eq. (1) cannot form the Wannier-Stark ladders, but appears to be periodic.

Next, we want to see the localization behavior in the case of external uniform fields of moderate strength. For briefness, we set the minimum energy to be $\epsilon_{\min} = 0$ (we can always add a constant shift on the chemical potential to achieve it. Meanwhile, such a process makes no changes to the localization). Given the integral form of Bessel functions, the non-Hermitian wave function φ_l as a function of β and w can be expressed as

$$\varphi_l(\beta, w) \propto \frac{1}{2\pi} \int_{-\pi}^{\pi} e^{i[(\tau - i\beta)l - \frac{2t_0}{\omega} \sin(\tau)]} d\tau. \quad (14)$$

Given the positive integer lattice index l, it can be implied from Eq. (14) that $\varphi_l(\beta, w)$ gains the largest value with the largest β ($e^{\beta} > 1$). To see how the strength of uniform fields affects $\varphi_l(\beta, w)$, we focus on

$$\frac{\partial \varphi_l(\beta, w)}{\partial w} \propto \left(-\frac{t_0}{w^2}\right) e^{\beta l} \left[Z_{l-1}\left(\frac{2t_0}{w}\right) - Z_{l+1}\left(\frac{2t_0}{w}\right)\right], \quad (15)$$

where $Z_l(x)$ is the $J_l(x)$ or $Y_l(x)$. The maximum $\varphi_l(\beta, w)$ can take place when

$$Z_{l-1}\left(\frac{2t_0}{w_c}\right) = Z_{l+1}\left(\frac{2t_0}{w_c}\right). \quad (16)$$

Equation (16) suggests that the critical w_c, where the maximal localization takes place, is dependent on the site index l and the net tunneling t_0. The analysis above coincides with the results in Fig. 2(a), where for the chain of finite size, different critical field strength w_c is observed with different fixed net tunneling t_0. Considering Eq. (15), it can be indicated that for $e^{\beta} > 1$, the asymmetric tunneling tends to have the physical states piled up at the end of the lattice $l = N$ (see the Appendix). For a given t_0, if the strength of the external uniform field satisfies $w < w_N$ and $Z_{N-1}(\frac{2t_0}{w_N}) = Z_{N+1}(\frac{2t_0}{w_N})$, the lattice-

end localization can be true. Otherwise, the uniform field can pull back the piled-up states in the case of finite lattice size. Numerically, in Fig. 2(b), for the chain of length $N = 5$, the maximal localization takes place at $l = 1$ with $w = 3$, instead of $l = N$ even though $e^{\beta} > 1$. Such results suggest that uniform fields can destroy the lattice-end localization induced by the NHSE for a chain of finite size. Meanwhile, in Fig. 2(c), when the length of the chain is enlarged and reset $\beta = 3$, it is observed that the NHSE gradually overcomes Wannier-Stark localization, retaking the dominant place.

B. Two-dimensional localization behavior

For two-dimensional lattice models ($d = 2$), we can have asymmetric tunneling in both the x and y directions. Also, the external uniform fields can be applied in arbitrary directions. First, we consider the lattice of square-shape boundaries and the Hamiltonian can be described by

$$
\begin{aligned}
H_{2d} = \sum_{m,n=1}^{N-1} & \left(t_x^R c_{m+1,n}^{\dagger} c_{m,n} + t_x^L c_{m,n}^{\dagger} c_{m+1,n}\right. \\
& \left. + t_y^U c_{m,n+1}^{\dagger} c_{m,n} + t_y^D c_{m,n}^{\dagger} c_{m,n+1}\right) \\
& + \sum_{m,n=1}^{N} (w_x m c_{m,n}^{\dagger} c_{m,n} + w_y n c_{m,n}^{\dagger} c_{m,n}), \quad (17)
\end{aligned}
$$

where $t_x^{R(L)}$ and $t_y^{U(D)}$ present the tunneling in the x, y directions towards the right (left), up (down) side. $w_{x(y)}$ depicts the strength of the external uniform field. Unlike the one-dimensional case, the wave functions in the two-dimensional model cannot be analytically obtained. However, the localization can be measured via a brute force method. In detail, the Hamiltonian in Eq. (17) can be expressed as $H_{2d} = \Phi^{\dagger} \tilde{h} \Phi$, $\Phi^{\dagger} = (c_{1,1}^{\dagger}, c_{1,2}^{\dagger}, \ldots, c_{1,N}^{\dagger}, \ldots, c_{N,1}^{\dagger}, \ldots, c_{N,N}^{\dagger})$ and $\tilde{h}$ can be diagonalized via

$$\tilde{\psi}^{-1} \tilde{h} \tilde{\psi} = D, \quad (18)$$

where D is a diagonal matrix consisting of entries of eigenenergies and $\tilde{\psi}$ is the eigenstate of the Hamiltonian. Correspondingly, the localization strength can be defined as $\rho = \tilde{\phi} \tilde{\psi}^*$, where $\tilde{\psi}^*$ is the complex conjugate of the state $\tilde{\psi}$.
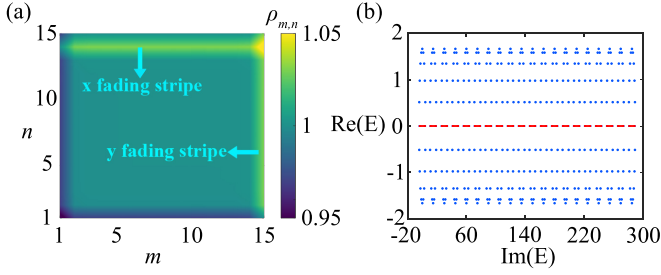
FIG. 3. (a) The fading stripe localization can be formed in both x and y directions with $t_{x0} = 2$, $t_{y0} = 2$, $e^{\beta_x} = 1.5$, $e^{\beta_y} = 1.5$, and $w_x = w_y = 15$. (b) The real-space energy spectrum with PBCs in the x direction and OBCs in the y direction (blue dots) does not coincide with the energy spectrum with OBCs in both x and y directions (red dots), indicating the existence of NHSE.

Specifically, the localization strength on the (m, n) site can be depicted by [71]

$$\rho_{m,n} = \sum_{r=1}^{N \times N} \tilde{\psi}^*[(m-1)N + n, r]\tilde{\psi}[(m-1)N + n, r]. \quad (19)$$

First, we consider the OBCs in both the x and y directions for the lattice of finite size. The asymmetric tunneling is assumed to be

$$t_L = t_{x0}e^{-\beta_x}, \qquad t_R = t_{x0}e^{\beta_x},$$
$$t_D = t_{y0}e^{-\beta_y}, \qquad t_U = t_{y0}e^{\beta_y}. \quad (20)$$

In the case of vanishing uniform fields and $e^{\beta_x} > 1$, $e^{\beta_y} > 1$, the states corresponding to all eigenenergies are supposed to be localized at the up-right corner regardless of the value of net tunneling t_{x0}, t_{y0}. This result stems from the two-dimensional NHSE. As we gradually turn on and enlarge the uniform field, it can be observed that with moderate field strength, although $\rho_{m,n}$ is maximally localized at the corner $x = N$, $y = N$, there still exist states of specific energies lying on other positions. According to the $\rho_{m,n}$ shown in Fig. 3(a), we prefer to name such a localization as the fading stripe localization. In Fig. 3(b), the energy spectrum obtained with OBCs in both the x and y directions is purely real, which does not coincide with the energy spectrum that is obtained with PBCs in the x direction and OBCs in the y direction, indicating the NHSE as an ingredient of the fading stripe localization. Analytically, the fading stripe localization can be conceived as a compromise between the two-dimensional NHSE and Wannier-Stark localization, where the corner modes get its tails pulled back by the uniform fields. According to the formation of Wannier-Stark ladders [58], it can be implied that the states of different energies are pulled back differently. When the strength of the uniform field is extremely large, the states of different energies are equally distributed at different sites and the corner localization induced by the two-dimensional NHSE is suppressed. At this stage, the fading stripe gradually becomes an equally distributed stripe.

The localization in non-Hermitian systems is extremely sensitive to the shapes of the boundaries. An illustration can be made by taking the diagonal-line boundaries, where the square lattices are cut into two triangles and the system, which we considered, is the upper blue shaded triangle schematically
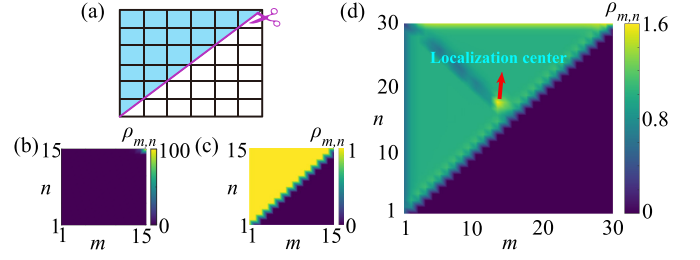

FIG. 4. (a) The schematic picture of the lattice with diagonal-line boundaries. The system, which we considered, lies in the upper blue shaded triangles. (b) With vanishing uniform fields and $e^{\beta_x} = e^{\beta_y} = 4$, $t_{x0} = t_{y0} = 2$, the corner-skin localization is observed. (c) With the absence of NHSE and $e^{\beta_x} = e^{\beta_y} = 1$, $w_x = w_y = 5$, the system possesses equally distributed localization. (d) With moderate field strength $w_x = w_y = 10$ and two-dimensional NHSE $e^{\beta_x} = e^{\beta_y} = 4$, the maximal localization center is a single point. Neither a fading stripe nor the corner localization is observed.

shown in Fig. 4(a). We demonstrate that, with the vanishing uniform fields, the corner-skin localization induced by the two-dimensional NHSE can still be observed [see Fig. 4(b)]. In the case of the large field limit, the NHSE is greatly suppressed and the states of different energies are equally distributed on the entire system with step-ladder boundaries, which is shown in Fig. 4(c). For the uniform fields of moderate strength and the presence of NHSE, $\rho_{m,n}$ has a single maximal localization center and no fading stripes or corner localization are observed [see Fig. 4(d)].

Although the shapes of the boundary are of great importance in non-Hermitian systems, a continuous shift in boundary conditions may not contribute to changes in the localization. An analytical illustration can be exhibited by considering the twisted boundary conditions (TBCs), where the tunneling towards the right (left) and up (down) side for sites at the boundaries can be described as

$$t_{\text{TBCs}}^R = t_x^R e^{i\theta_x}c_{1,j}^\dagger c_{N,j}, \qquad t_{\text{TBCs}}^L = t_x^L e^{-i\theta_x}c_{N,j}^\dagger c_{1,j},$$
$$t_{\text{TBCs}}^U = t_y^U e^{i\theta_y}c_{j,1}^\dagger c_{j,N}, \qquad t_{\text{TBCs}}^D = t_y^D e^{-i\theta_y}c_{j,N}^\dagger c_{j,1}, \quad (21)$$

where $j \in [1, N]$ and $\theta_{x(y)}$ is the torsion number. Specifically, for $\theta_{x(y)} = 2p\pi$, $p \in Z$, TBCs coincide with PBCs. For $\theta_{x(y)} = (2p+1)\pi$, $p \in Z$, TBCs coincide with the anti-PBCs. It should be pointed out that applying the TBCs has the same effect as inserting the magnetic fluxes and correspondingly a phase factor can be attached to the cell function $c_{i,j} \to c_{i,j}e^{i\phi_{i,j}R_{i,j}}$. It shall be kept as

$$\phi_{N,j}R_{N,j} - \phi_{1,j}R_{1,j} = \theta_x,$$
$$\phi_{j,N}R_{j,N} - \phi_{j,1}R_{j,1} = \theta_y. \quad (22)$$

With the absence of external uniform fields and given $\phi_{i,j} = \phi$ for $\forall i, j \in [1, N]$, the system possesses discrete translational symmetry. Now the momentum k can be well defined. The effects of TBCs (the same as applying the magnetic flux) can be canceled by a shift of the momentum $k' = k + \phi$, and similarly the generalized Bloch wave vector $\tilde{\beta}'_{x(y)} = k - i\beta_{x(y)} + \phi$. We notice that the NHSE localization can be identified by the radius of the generalized Brillouin zone [$e^{\beta_{x,y}} < (>)1$]. A shift by the real phase in the generalized Bloch wave vector will not change the radius of the generalized Brillouin zone. Hence,

continuously tuning the torsion number $\theta_{x(y)}$ of TBCs in non-Hermitian systems with asymmetric tunneling will contribute no differences to the localization behavior. Considering the PBCs where we have $\theta_{x(y)} = 2p\pi$, we can posit that the NHSE will not take place when the TBCs are applied, despite the absence of uniform fields.

C. Effects of uniform fields on the exceptional points

In non-Hermitian quantum chains, there are cases that, with the changing of parameters, the degenerate states are collapsing into one exceptional point (EP) and the matrix of the Hamiltonian becomes nondiagonalizable [48,72–86]. Now, we reveal how EPs are affected by the uniform fields. To achieve EPs in lattice models, we should typically obtain multiple bands at first, which can be realized by including sublattices, spins, or higher orbitals. Here, we consider a modified version of the non-Hermitian bipartite chain in Ref. [72] with the uniform fields included. For completeness, the Hamiltonian can be given as

$$\hat{H} = \sum_{n=1}^{N-1} \left[\frac{r}{2}(c_n^\dagger d_{n+1} + d_n^\dagger c_{n+1}) + \frac{ir}{2}(c_{n+1}^\dagger c_n \right.$$

$$- d_{n+1}^\dagger d_n) + \text{H.c.} \left] + \sum_{n=1}^{N} \left[v(c_n^\dagger d_n + d_n^\dagger c_n) \right.$$

$$+ \left(\frac{i\gamma}{2} + wn \right) c_n^\dagger c_n - \frac{i\gamma}{2} d_n^\dagger d_n \right) \right], \tag{23}$$

where v is the intracell tunneling and $\frac{ir}{2}(\frac{r}{2})$ denotes the intercell tunneling between the same (different) sublattices. w depicts the strength of the uniform field on the sublattice. Here, non-Hermiticity lies in the nonzero γ, which is also set as the unit of energy. With the vanishing uniform fields, the system is PT symmetric, where the parity symmetry operator is $P : \bigoplus_n \sigma_x^n$ and the time-reversal symmetry can be described as the complex conjugate operator. With the changing of the intracell tunneling v, the system will encounter a transition from the parity-time symmetry broken phase to the unbroken phase at $v_0 = 0.5\gamma$, where two high-order EPs at $\epsilon = \pm r$, as well as an EP at $\epsilon = 0$, are present [see Fig. 5(a)]. Meanwhile, the imaginary part of the eigenenergy will disappear at v_0 as a consequence of the phase transition [see Fig. 5(b)]. The nonzero uniform field will lead to a site-dependent shift on the local potential and break the parity-time symmetry. In addition, the uniform fields will force the Hamiltonian matrix of Eq. (23) to be full rank. Considering the discussion above, we can posit that the uniform fields will destroy the formation of EPs. The numerical results in Figs. 5(c) and 5(d) show a sound agreement, where, unlike the field-absent case, changing the value of v, the system will not have any critical points, where the imaginary part of the energy spectrum starts to disappear and no EPs are observed.

III. PROPOSALS ON THE EXPERIMENTAL SIMULATION

An experimental proposal to simulate the Hamiltonian in Eq. (1) can be achieved by the electrical circuit lattices. We shall point out that, although the electrical circuits are classical systems, its Laplacian can be of the same expression as the matrix form of the Hamiltonian. Such methods were extensively used to synthesize lattice models [87–97].
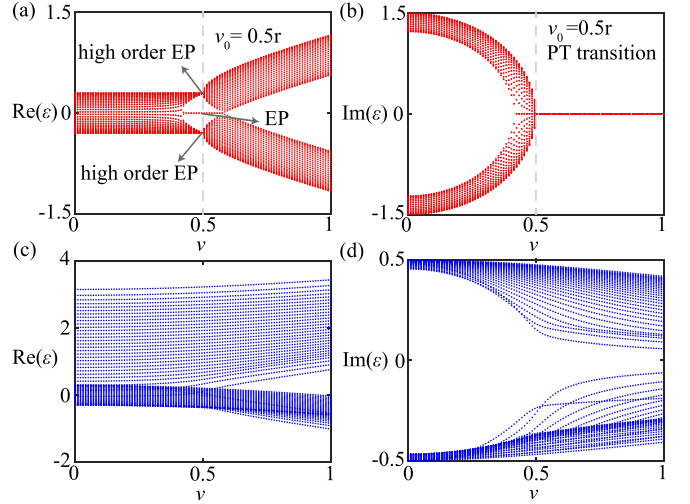

FIG. 5. (a) With the vanishing external uniform fields and $r = 0.3\gamma$, there exist two high-order EPs and a single EP with $v_0 = 0.5\gamma$. (b) The phase transition from parity-time symmetry broken phase to the unbroken phase takes place at $v_0 = 0.5\gamma$, where the imaginary part of the energy spectrum starts to disappear. (c) No EPs are observed with nonzero uniform fields $w = 0.1$. (d) The uniform fields will break the parity-time symmetry and the imaginary part of the energy spectrum always exists.

The schematic picture of our experimental setup is shown in Fig. 6. Physically, each node is connected to the ground and a voltage $V(t) = V(0)e^{i\omega t}$ is applied. The current flowing in the jth node of the circuit lattice can be governed by the Kirchhoff law

$$I_j = \sum_i L_{ij} V_j, \tag{24}$$

where V_j is is the electrical potential on the jth node and L_{ij} depicts the net impedance of all the electrical elements linked to the node j. Conventionally, L_{ij} is named as the circuit Laplacian and is decided by the structure of the circuit lattice. Specifically, for our setups, I_j can be given by

$$I_j = \frac{1}{\tilde{R}_j} V_j + (i\omega C + R_{OA})(V_j - V_{j+1})$$

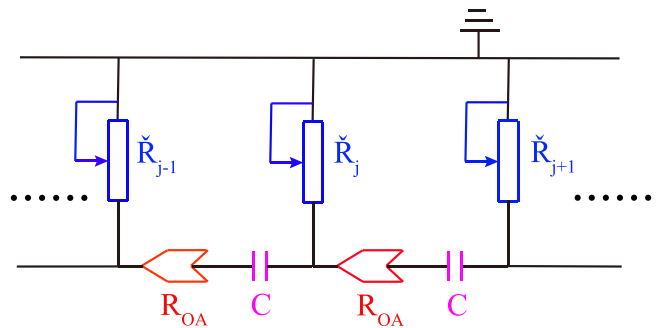$$+ (i\omega C - R_{OA})(V_j - V_{j-1}), \tag{25}$$

FIG. 6. The experimental setup of circuit lattices to simulate the Hamiltonian of the non-Hermitian chain with asymmetric tunneling and uniform fields.

where $\breve{R}_j$ is the slide-wire rheostat, whose impedance is set to be site dependent, $\tilde{R}_j = \frac{1}{j}R_0$. $i\omega C$ is the impedance of the capacitor. Here, the nonreciprocal asymmetric tunneling is realized via the operational amplifier R_{OA}, which serves as the negative impedance converter with current inversion (INIC). Specifically, for the current flowing from the right side, the impedance of R_{OA} is negative. While for the current flowing from the opposite direction, the sign of the impedance of R_{OA} reverses. The details of the structure of INIC can be found in Ref. [91]. The exact form of the circuit Laplacian can be written as $L_{ij} =$

$$\begin{bmatrix} \frac{1}{R_0} + s & -i\omega C - R_{OA} & 0 & \dots \\ -i\omega C + R_{OA} & \frac{2}{R_0} + s & -i\omega C - R_{OA} & \dots \\ 0 & -i\omega C + R_{OA} & \frac{3}{R_0} + s & \dots \\ \dots & & & \end{bmatrix},$$

(26)

where the term proportional to the identify matrix I with the coefficient $s = 2i\omega C$ can be dropped out. In correspondence to the Hamiltonian in Eq. (1), the parameters for the circuit lattices are set as

$$\frac{1}{R_0} = w, \quad R_{OA} = \frac{t_R - t_L}{2}, \quad C = \frac{i(t_L + t_R)}{2\omega}. \quad (27)$$

To the end of this part, it should be mentioned that the experimental setup above serves as an illustrative presentation, and to achieve more complicated tunneling we add inductors or resistors parallelized to the capacitor C.

IV. CONCLUSION

We demonstrate the localization behavior for non-Hermitian tightly bound states with asymmetric tunneling and uniform fields in one and two dimensions. We exhibit that the NHSE can still exist in the systems without discrete translational symmetry and show how the NHSE competes with Wannier-Stark localization in various dimensions. Specifically, for two-dimensional systems with square-shaped boundaries, the fading stripe localization is observed. In addition, as we change the square lattice to a triangle one with the diagonal-line boundary, the localization changes dramatically. Once taking the twisted boundary conditions, we prove that a continuous tuning of the torsion number can not affect the localization and correspondingly the NHSE will be absent. Apart from the localization, it is also shown that the uniform fields will break the *PT* symmetry and destroy the formation of EPs. In the end, an experimental simulation of the non-Hermitian chain with uniform fields is proposed via the electrical circuit lattices.

APPENDIX: NON-HERMITIAN SKIN EFFECTS INDUCED BY THE ASYMMETRIC TUNNELING

In non-Hermitian systems, the asymmetric tunneling can induce the NHSE and get the states piled up at one end of the lattice. An illustration can be shown via the transfer matrix. Here we briefly review this method. First, the one-dimensional chain with asymmetric tunneling can be depicted by

$$H = \sum_{j=1}^{N-1} (t_R c_{j+1}^\dagger c_j + t_L c_j^\dagger c_{j+1}). \quad (A1)$$

Given the one-particle state $\psi = \sum_l \gamma_l^\dagger |0\rangle$, the Schrödinger equation can lead to the recurrence formula

$$t_R \gamma_{l-1} + t_L \gamma_{l+1} = E\gamma_l. \quad (A2)$$

The transfer matrix T can be given via

$$\begin{pmatrix} \gamma_{l+1} \\ \gamma_l \end{pmatrix} = T \begin{pmatrix} \gamma_l \\ \gamma_{l-1} \end{pmatrix} = T^{l-1} \begin{pmatrix} \gamma_2 \\ \gamma_1 \end{pmatrix}, \quad (A3)$$

$$T = \begin{pmatrix} \frac{E}{t_L} & -\frac{t_R}{t_L} \\ 1 & 0 \end{pmatrix}. \quad (A4)$$

We add a constant shift on the chemical potential and only focus on the localization of the state with $E = 0$. Now the transfer matrix T only contains the off-diagonal entries and we have

$$T^{2N} = (-t_R/t_L)^N I, \quad T^{2N+1} = (-t_R/t_L)^N T, \quad (A5)$$

where I is the identity matrix. Hence, for $t_R/t_L = e^{2\beta} > (<)1$, the states are localized at the right (left) end of the lattice, which only describes the NHSE. A similar conclusion was obtained in Ref. [67], where the NHSE was identified via $|\det(T)| \neq 1$. When the uniform fields are considered, the transfer matrix changes to the following form:

$$T' = (t_L)^{-1} \begin{pmatrix} E - wl & -t_R \\ t_L & 0 \end{pmatrix}. \quad (A6)$$

In the case of the thermodynamic limit $N \to \infty$, we concentrate on the dominant term proportional to l^N, which is the (1,1) entry of the $(T')^N$. Specifically, we have

$$T'^{2N}_{(1,1)} = (t_L)^{-2N}(E - wl)^{2N} \left[1 - (2N - 1)\frac{t_R t_L}{(E - wl)^2} \right.$$
$$\left. + \cdots (-1)^N \frac{(t_R t_L)^N}{(E - wl)^{2N}} \right],$$
$$T'^{2N+1}_{(1,1)} = (t_L)^{-(2N+1)}(E - wl)^{2N+1} \left[1 - (2N)\frac{t_R t_L}{(E - wl)^2} \right.$$
$$\left. + \cdots + (-1)^N(N + 1)\frac{(t_R t_L)^N}{(E - wl)^{2N}} \right]. \quad (A7)$$

From Eq. (A7), it can be inferred that, unlike the transfer matrix in Eq. (A5), we cannot simply identify the localization behavior via the asymmetric tunneling $t_{R(L)}$. However, due to the special recurrence properties, we gain the analytical form of the wave functions.

[1] N. Hatano and D. R. Nelson, Vortex pinning and non-hermitian quantum mechanics, Phys. Rev. B **56**, 8651 (1997).

[2] C. M. Bender, M. V. Berry, and A. Mandilara, Generalized pt symmetry and real spectra, J. Phys. A: Math. Gen. **35**, L467 (2002).

[3] C. M. Bender, Pt-symmetric quantum theory, J. Phys.: Conf. Ser. **631**, 012002 (2015).

[4] K. Kawabata, K. Shiozaki, and S. Ryu, Topological Field Theory of Non-Hermitian Systems, Phys. Rev. Lett. **126**, 216405 (2021).

[5] Z. Gong, Y. Ashida, K. Kawabata, K. Takasan, S. Higashikawa, and M. Ueda, Topological Phases of Non-Hermitian Systems, Phys. Rev. X **8**, 031079 (2018).

[6] D. S. Borgnia, A. J. Kruchkov, and R.-J. Slager, Non-Hermitian Boundary Modes and Topology, Phys. Rev. Lett. **124**, 056802 (2020).

[7] H.-Y. Wang, X.-M. Zhao, L. Zhuang, and W.-M. Liu, Non-floquet engineering in periodically driven dissipative open quantum systems, J. Phys.: Condens. Matter **34**, 365402 (2022).

[8] E. Edvardsson, F. K. Kunst, and E. J. Bergholtz, Non-hermitian extensions of higher-order topological phases and their biorthogonal bulk-boundary correspondence, Phys. Rev. B **99**, 081302(R) (2019).

[9] L. Xiao, T. Deng, K. Wang, G. Zhu, Z. Wang, W. Yi, and P. Xue, Non-hermitian bulk-boundary correspondence in quantum dynamics, Nat. Phys. **16**, 761 (2020).

[10] T. Li, J.-Z. Sun, Y.-S. Zhang, and W. Yi, Non-bloch quench dynamics, Phys. Rev. Res. **3**, 023022 (2021).

[11] K. Yokomizo and S. Murakami, Non-Bloch Band Theory of Non-Hermitian Systems, Phys. Rev. Lett. **123**, 066404 (2019).

[12] K. Kawabata, S. Higashikawa, Z. Gong, Y. Ashida, and M. Ueda, Topological unification of time-reversal and particle-hole symmetries in non-hermitian physics, Nat. Commun. **10**, 297 (2019).

[13] H. Shen, B. Zhen, and L. Fu, Topological Band Theory for Non-Hermitian Hamiltonians, Phys. Rev. Lett. **120**, 146402 (2018).

[14] W.-T. Xue, Y.-M. Hu, F. Song, and Z. Wang, Non-Hermitian Edge Burst, Phys. Rev. Lett. **128**, 120401 (2022).

[15] X.-R. Wang, C.-X. Guo, and S.-P. Kou, Defective edge states and number-anomalous bulk-boundary correspondence in non-hermitian topological systems, Phys. Rev. B **101**, 121116(R) (2020).

[16] K. Yamamoto, M. Nakagawa, K. Adachi, K. Takasan, M. Ueda, and N. Kawakami, Theory of Non-Hermitian Fermionic Superfluidity with a Complex-Valued Interaction, Phys. Rev. Lett. **123**, 123601 (2019).

[17] S. Longhi, Non-hermitian skin effect and self-acceleration, Phys. Rev. B **105**, 245143 (2022).

[18] F. K. Kunst, E. Edvardsson, J. C. Budich, and E. J. Bergholtz, Biorthogonal Bulk-Boundary Correspondence in Non-Hermitian Systems, Phys. Rev. Lett. **121**, 026808 (2018).

[19] L. Li, C. H. Lee, S. Mu, and J. Gong, Critical non-Hermitian skin effect, Nat. Commun. **11**, 5491 (2020).

[20] S. Longhi, Probing non-hermitian skin effect and non-bloch phase transitions, Phys. Rev. Res. **1**, 023013 (2019).

[21] K.-I. Imura and Y. Takane, Generalized bulk-edge correspondence for non-hermitian topological systems, Phys. Rev. B **100**, 165430 (2019).

[22] Y.-X. Xiao and C. T. Chan, Topology in non-hermitian chern insulators with skin effect, Phys. Rev. B **105**, 075128 (2022).

[23] R. Sarkar, S. S. Hegde, and A. Narayan, Interplay of disorder and point-gap topology: Chiral modes, localization, and non-hermitian anderson skin effect in one dimension, Phys. Rev. B **106**, 014207 (2022).

[24] M. Žnidarič, Solvable non-Hermitian skin effect in many-body unitary dynamics, Phys. Rev. Res. **4**, 033041 (2022).

[25] Q. Liang, D. Xie, Z. Dong, H. Li, H. Li, B. Gadway, W. Yi, and B. Yan, Dynamic Signatures of Non-Hermitian Skin Effect and Topology in Ultracold Atoms, Phys. Rev. Lett. **129**, 070401 (2022).

[26] M. Lu, X.-X. Zhang, and M. Franz, Magnetic Suppression of Non-Hermitian Skin Effects, Phys. Rev. Lett. **127**, 256402 (2021).

[27] S. Longhi, Unraveling the non-Hermitian skin effect in dissipative systems, Phys. Rev. B **102**, 201103(R) (2020).

[28] F. Alsallom, L. Herviou, O. V. Yazyev, and M. Brzezińska, Fate of the non-hermitian skin effect in many-body fermionic systems, Phys. Rev. Res. **4**, 033122 (2022).

[29] N. Okuma, K. Kawabata, K. Shiozaki, and M. Sato, Topological Origin of Non-Hermitian Skin Effects, Phys. Rev. Lett. **124**, 086801 (2020).

[30] F. Schindler and A. Prem, Dislocation non-Hermitian skin effect, Phys. Rev. B **104**, L161106 (2021).

[31] F. Song, S. Yao, and Z. Wang, Non-Hermitian Skin Effect and Chiral Damping in Open Quantum Systems, Phys. Rev. Lett. **123**, 170401 (2019).

[32] X. Zhang, Y. Tian, J. Jiang, M. Lu, and Y. Chen, Observation of higher-order non-hermitian skin effect, Nat. Commun. **12**, 5377 (2021).

[33] S. Longhi, Non-Hermitian skin effect beyond the tight-binding models, Phys. Rev. B **104**, 125109 (2021).

[34] Y. Yi and Z. Yang, Non-Hermitian Skin Modes Induced by On-Site Dissipations and Chiral Tunneling Effect, Phys. Rev. Lett. **125**, 186802 (2020).

[35] L. Zhang, Y. Yang, Y. Ge, Y. Guan, Q. Chen, Q. Yan, R. Xi, Y. Li, D. Jia, S. Yuan, H. Sun, H. Chen, and B. Zhang, Acoustic non-Hermitian skin effect from twisted winding topology, Nat. Commun. **12**, 6297 (2021).

[36] S. Yao, F. Song, and Z. Wang, Non-Hermitian Chern Bands, Phys. Rev. Lett. **121**, 136802 (2018).

[37] K. Kawabata, M. Sato, and K. Shiozaki, Higher-order non-Hermitian skin effect, Phys. Rev. B **102**, 205118 (2020).

[38] S. Longhi, Self-Healing of Non-Hermitian Topological Skin Modes, Phys. Rev. Lett. **128**, 157601 (2022).

[39] K. Yokomizo and S. Murakami, Non-bloch band theory in bosonic bogoliubov–de gennes systems, Phys. Rev. B **103**, 165123 (2021).

[40] Z. Yang, K. Zhang, C. Fang, and J. Hu, Non-Hermitian Bulk-Boundary Correspondence and Auxiliary Generalized Brillouin Zone Theory, Phys. Rev. Lett. **125**, 226402 (2020).

[41] S. Yao and Z. Wang, Edge States and Topological Invariants of Non-Hermitian Systems, Phys. Rev. Lett. **121**, 086803 (2018).

[42] Y. Kazuki and M. Shuichi, Non-bloch band theory and bulk-edge correspondence in non-hermitian systems, Prog. Theor. Exp. Phys. **2020**, 12A102 (2020).

[43] W.-T. Xue, M.-R. Li, Y.-M. Hu, F. Song, and Z. Wang, Simple formulas of directional amplification from non-bloch band theory, Phys. Rev. B **103**, L241408 (2021).

[44] K. Kawabata, N. Okuma, and M. Sato, Non-bloch band theory of non-hermitian hamiltonians in the symplectic class, Phys. Rev. B **101**, 195147 (2020).

[45] F. Song, S. Yao, and Z. Wang, Non-Hermitian Topological Invariants in Real Space, Phys. Rev. Lett. **123**, 246801 (2019).

[46] L.-J. Lang, Y. Weng, Y. Zhang, E. Cheng, and Q. Liang, Dynamical robustness of topological end states in nonreciprocal su-schrieffer-heeger models with open boundary conditions, Phys. Rev. B **103**, 014302 (2021).

[47] S. Longhi, Non-Bloch-Band Collapse and Chiral Zener Tunneling, Phys. Rev. Lett. **124**, 066602 (2020).

[48] L. Xiao, T. Deng, K. Wang, Z. Wang, W. Yi, and P. Xue, Observation of Non-Bloch Parity-Time Symmetry and Exceptional Points, Phys. Rev. Lett. **126**, 230402 (2021).

[49] K. Zhang, Z. Yang, and C. Fang, Correspondence between Winding Numbers and Skin Modes in Non-Hermitian Systems, Phys. Rev. Lett. **125**, 126402 (2020).

[50] K. Zhang, Z. Yang, and c. Fang, Universal non-hermitian skin effect in two and higher dimensions, Nat. Commun. **13**, 2496 (2022).

[51] K.-M. Kim and M. J. Park, Disorder-driven phase transition in the second-order non-hermitian skin effect, Phys. Rev. B **104**, L121101 (2021).

[52] A. K. Ghosh and T. Nag, Non-hermitian higher-order topological superconductors in two dimensions: Statics and dynamics, Phys. Rev. B **106**, L140303 (2022).

[53] L. C. Xie, H. C. Wu, X. Z. Zhang, L. Jin, and Z. Song, Two-dimensional anisotropic non-hermitian lieb lattice, Phys. Rev. B **104**, 125406 (2021).

[54] Y. Fu, J. Hu, and S. Wan, Non-Hermitian second-order skin and topological modes, Phys. Rev. B **103**, 045420 (2021).

[55] X.-W. Luo and C. Zhang, Higher-Order Topological Corner States Induced by Gain and Loss, Phys. Rev. Lett. **123**, 073601 (2019).

[56] M. Ezawa, Non-hermitian higher-order topological states in nonreciprocal and reciprocal systems with their electric-circuit realization, Phys. Rev. B **99**, 201411(R) (2019).

[57] T. Liu, Y.-R. Zhang, Q. Ai, Z. Gong, K. Kawabata, M. Ueda, and F. Nori, Second-Order Topological Phases in Non-Hermitian Systems, Phys. Rev. Lett. **122**, 076801 (2019).

[58] H. Fukuyama, R. A. Bari, and H. C. Fogedby, Tightly bound electrons in a uniform electric field, Phys. Rev. B **8**, 5579 (1973).

[59] N. Hatano and D. R. Nelson, Localization Transitions in Non-Hermitian Quantum Mechanics, Phys. Rev. Lett. **77**, 570 (1996).

[60] F. Hebert, M. Schram, R. T. Scalettar, W. B. Chen, and Z. Bai, Hatano-nelson model with a periodic potential, Eur. Phys. J. B **79**, 465 (2011).

[61] S.-B. Zhang, M. M. Denner, T. Bzdušek, M. A. Sentef, and T. Neupert, Symmetry breaking and spectral structure of the interacting hatano-nelson model, Phys. Rev. B **106**, L121102 (2022).

[62] D. Emin and C. F. Hart, Existence of wannier-stark localization, Phys. Rev. B **36**, 7353 (1987).

[63] J. Zak, Stark Ladder in Solids? Phys. Rev. Lett. **20**, 1477 (1968).

[64] G. H. Wannier, Stark ladder in solids? a reply, Phys. Rev. **181**, 1364 (1969).

[65] J. Zak, Stark ladder in solids? a reply to a reply, Phys. Rev. **181**, 1366 (1969).

[66] X. Zhao, Existence of wannier-stark localization for the bloch electron on coupled chains in a uniform magnetic field and a uniform electric field, Phys. Lett. A **153**, 381 (1991).

[67] F. K. Kunst and V. Dwivedi, Non-hermitian systems and topology: A transfer-matrix perspective, Phys. Rev. B **99**, 245116 (2019).

[68] X. Luo, T. Ohtsuki, and R. Shindou, Transfer matrix study of the anderson transition in non-hermitian systems, Phys. Rev. B **104**, 104203 (2021).

[69] T. Mizoguchi and T. Koma, Bulk-edge correspondence in two-dimensional topological semimetals: A transfer matrix study of antichiral edge modes, Phys. Rev. B **103**, 195310 (2021).

[70] In the conventional Peierls substitution, the flux quanta per two-dimensional plaquette, $\phi = \frac{1}{2\pi}(\theta_{i,j}^x + \theta_{i+1,j}^y - \theta_{i,j+1}^x - \theta_{i,j}^y)$, is real and can be absorbed by artificially adding a real phase in the cell wave function. In non-Hermitian systems, the asymmetry in tunneling can be canceled by adding a complex phase in the jth cell wave function, $\Psi_j' = e^{i(-i\beta j)}\Psi_j$.

[71] The localization in Eq. (19) can also gain a similar definition in the one-dimensional case and the localization strength on the ith site of a quantum chain is $\rho_i = \sum_{r=1}^N \tilde{\psi}^*(i,r)\tilde{\psi}(i,r)$.

[72] T. E. Lee, Anomalous Edge State in a Non-Hermitian Lattice, Phys. Rev. Lett. **116**, 133903 (2016).

[73] W. D. Heiss, The physics of exceptional points, J. Phys. A: Math. Theor. **45**, 444016 (2012).

[74] N. Hadiseh, L.-G. Gisela, H. E. Lopez-Aviles, S. Alexander, A. U. Hassan, Z. Qi, R. Stefan, L. Patrick, D. N. Christodoulides, and K. Mercedeh, Observation of chiral state transfer without encircling an exceptional point, Nature (London) **605**, 256 (2022).

[75] M. Mohammad-Ali and A. Andera, Exceptional points in optics and photonics, Science **363**, eaar7709 (2019).

[76] H. Dieter, Circling exceptional points, Nat. Phys. **12**, 823 (2016).

[77] K. Kawabata, T. Bessho, and M. Sato, Classification of Exceptional Points and Non-Hermitian Topological Semimetals, Phys. Rev. Lett. **123**, 066405 (2019).

[78] P. Djorwe, Y. Pennec, and B. Djafari-Rouhani, Exceptional Point Enhances Sensitivity of Optomechanical Mass Sensors, Phys. Rev. Appl. **12**, 024002 (2019).

[79] P. Jun-Hee, N. Abdoulaye, C. Wei, H. Liyi, K. Ashok, L. Thomas, L. Yu-Hwa, and K. Boubacar, Symmetry-breaking-induced plasmonic exceptional points and nanoscale sensing, Nat. Phys. **16**, 462 (2020).

[80] S. K. Ozdemir, S. Rotter, F. Nori, and L. Yang, Parity-time symmetry and exceptional points in photonics, Nat. Mater. **18**, 783 (2019).

[81] W. Liu, Y. Wu, C.-K. Duan, X. Rong, and J. Du, Dynamically Encircling an Exceptional Point in a Real Quantum System, Phys. Rev. Lett. **126**, 170506 (2021).

[82] S. Ramezanpour and A. Bogdanov, Tuning exceptional points with kerr nonlinearity, Phys. Rev. A **103**, 043510 (2021).

[83] A. Krasnok, N. Nikita, and A. Alù, Parity-time symmetry and exceptional points: A tutorial, in *IEEE Antennas and Propagation Magazine*, Vol. 63 (IEEE, 2021), pp. 110–121.

[84] L. Ge, Anomalous parity-time–symmetry transition away from an exceptional point, Phys. Rev. A **94**, 013837 (2016).

[85] I. Mandal and E. J. Bergholtz, Symmetry and Higher-Order Exceptional Points, Phys. Rev. Lett. **127**, 186601 (2021).

[86] Y. N. Joglekar and A. K. Harter, Passive parity-time-symmetry-breaking transitions without exceptional points in dissipative photonic systems, Photonics Research **6**, A51 (2018).

[87] Q.-B. Zeng and Y. Xu, Winding numbers and generalized mobility edges in non-hermitian systems, Phys. Rev. Res. **2**, 033052 (2020).

[88] Q.-B. Zeng, Y.-B. Yang, and Y. Xu, Higher-order topological insulators and semimetals in generalized aubry-andré-harper models, Phys. Rev. B **101**, 241104(R) (2020).

[89] T. Hofmann, T. Helbig, C. H. Lee, M. Greiter, and R. Thomale, Chiral Voltage Propagation and Calibration in a Topolectrical Chern Circuit, Phys. Rev. Lett. **122**, 247702 (2019).

[90] E. Zhao, Topological circuits of inductors and capacitors, Ann. Phys. (NY) **399**, 289 (2018).

[91] C. H. Lee, S. Imhof, C. Berger, F. Bayer, J. Brehm, L. W. Molenkamp, T. Kiessling, and R. Thomale, Topolectrical circuits, Commun. Phys. **1**, 39 (2018).

[92] M. Ezawa, Braiding of majorana-like corner states in electric circuits and its non-hermitian generalization, Phys. Rev. B **100**, 045407 (2019).

[93] S. Li, R. Shao, L. Zhang, O. You, Y. Xiang, T. Cui, and S. Zhang, Non-hermitian skin effect in a non-hermitian electrical circuit, Research **2021**, 5608038 (2021).

[94] Q.-B. Zeng and R. Lü, Evolution of spectral topology in one-dimensional long-range nonreciprocal lattices, Phys. Rev. A **105**, 042211 (2022).

[95] T. Bzdušek and J. Maciejko, Flat bands and band-touching from real-space topology in hyperbolic lattices, Phys. Rev. B **106**, 155146 (2022).

[96] A. Stegmaier, L. K. Upreti, R. Thomale, and I. Boettcher, Universality of Hofstadter Butterflies on Hyperbolic Lattices, Phys. Rev. Lett. **128**, 166402 (2022).

[97] M. Di Ventra, Y. V. Pershin, and C.-C. Chien, Custodial Chiral Symmetry in a Su-Schrieffer-Heeger Electrical Circuit with Memory, Phys. Rev. Lett. **128**, 097701 (2022).